Colloids and Surfaces B: Biointerfaces 161 (2018) 628–635

Contents lists available at ScienceDirect

Colloids and Surfaces B: Biointerfaces

journal homepage: www.elsevier.com/locate/colsurfb

Full Length Article

Fabricating hierarchical micro and nano structures on implantable Co–Cr–Mo alloy for tissue engineering by one-step laser ablation

Liguo Qin[a,*], Hongxing Wu[a], Junde Guo[a], Xinan Feng[a], Guangneng Dong[a], Jinyou Shao[b], Qunfeng Zeng[a], Yali Zhang[c,*], Yuanbin Qin[d]

[a] Key Laboratory of Education Ministry for Modern design & Rotary-Bearing System, Xi'an Jiaotong University, Xi'an, 710049, PR China
[b] Micro and Nanotechnology Research Center, State Key Laboratory for Manufacturing Systems Engineering, Xi'an Jiaotong University, Xi'an, 710049, China
[c] Key Laboratory of Biomedical Information Engineering of Ministry of Education, School of Life Science and Technology, Xi'an Jiaotong University, Xi'an, 710049, PR China
[d] Center for Advancing Materials Performance from the Nanoscale, State Key Laboratory for Mechanical Behavior of Materials, Xi'an Jiaotong University, Xi'an 710049, PR China

ARTICLE INFO

Article history:
Received 20 July 2017
Received in revised form 18 October 2017
Accepted 7 November 2017
Available online 16 November 2017

Keywords:
Co–Cr–Mo alloy
Hierarchical structure
Bioactivity
Cell orientation

ABSTRACT

Surface texturing is one of the effective strategies to improve bioactivity of implantable materials. In this study, hierarchical micro and nano structure (HMN) were fabricated on Co–Cr–Mo alloy substrate by a movable picosecond laser irradiation. Respectively, microgrooves with nano ripples and islands were produced on Co–Cr–Mo alloy by low and high laser power density. X-ray diffraction apparatus (XRD) phase analysis illustrated that substrate was in the phase of γ- face-centered cubic structure (FCC) before laser treatment, while it was in ε-hexagonal closest packing structure (HCP) phase dominant after laser treatment. Cell adhesion and proliferation studies showed that the HMN surface exhibits enhanced adhesion of MC3TC-E1 osteoblast and promoted cell activity. Analyzing of the morphology of osteoblast cells indicated cells were in high ratio of elongation on the HMN surface, while they mainly kept in round shape on the polished surface. Results indicated the formation of hierarchical structure on Co–Cr–Mo alloy was able to improve biological performances, suggesting the potential application in cobalt based orthopedic implants.

1. Introduction

Nowadays, the number of patients who are suffering from trauma, congenital malformation and degenerative diseases is increasing. Fortunately, new biological therapeutics applications, such as regenerative medicine and tissue engineering, are promising ways to treat these diseases. It was reported that biomaterials played a pivotal role to guide new tissue formation in tissue engineering. Fabricating the substance that can provide best cellular microenvironment/interface for cell accommodation is the final goal [1,2]. The cobalt and its alloys, commonly used Co–Cr–Mo alloy, are ideal biomaterials for orthopedic and dental implants in recent years. It is owing to their high performance of wear and corrosion resistance [3–7]. However, the bulk ingredient of Co–Cr–Mo alloy is chemical inertness, which makes it more difficult to be modified. When these implants were transplanted in the human body, problems in inducing new bone/tissue formation have been aroused a lot of attentions. It has been found aseptic loosening was attributed to the main mechanism of hip joint replacement failure over 35 years, but no satisfactory solution has been found to date. Due to the recent attempts of less wear on articulating surfaces, focusing on the implant/bone interface has been increased [8]. In the previous study, layer-by-layer deposition technique was used to graft chitosan molecules on Co–Cr–Mo alloys to improve the biocompatibility [9]. The fabricating process was complicated and several steps were necessary. Designing and fabricating the micro and nano scale topography, called surface texturing, was an alternative way and has tremendous technological importance. The surface area was enhanced for the formation of various micro and nano structures. The textured surface has broad applications, such as improving cell growth and cell proliferation for biomedical implants [10], enhancing light trapping behaviors in optical usage and altering the surface wetting properties for self-cleaning performance [11,12].

Specially, increasing studies have been showed that surface texturing can be effective and mentioned as a promising way for

* Corresponding authors.
E-mail addresses: liguoqin@xjtu.edu.cn (L. Qin), yarlee@163.com (Y. Zhang).

https://doi.org/10.1016/j.colsurfb.2017.11.040
0927-7765/

solving loosening failure and the long-term success of the implant [13]. The final cell adhesion was depended on initial interaction between biomolecule and substrate, which played an important role in the fate of cells. So far several types of surface texture, such as fibers, grooves and pits at the nano and micro scale, were fabricated on various materials. The cell adhesion, shape, gene expression and differentiation were investigated by several researchers [14–17]. Amongst, Lu showed that the micro grooves (groove width from 4 to 40 μm), in the range of 0.5–2 fold of cell size, are more effective in guiding the cell orientation [17]. However, others showed that surfaces structured with 40–160 nm diameter nano-dots or nano grooves had better proliferation of osteoblast-like cells and an increase of focal adhesions [18,19]. Thus, hierarchical micro and nano (HMN) structuring orthopedic implants at two dimensions may be a fascinating strategy for achieving fast and stable fixation due to the synergetic effect of micro- and nano-scale surface roughness with surrounding tissues. However, few researches reported the effect of micro and nano structures on cell behaviors in implantable cobalt alloys. It was mainly restrained by the fabrication techniques for inducing defined patterns on the cobalt alloy surfaces. The laser fabrication provides both suitable surface topography and less surface contamination as compared with other methods. Another advantage of laser technique is texturing implants with more complicated patterns [20]. More recently, with advent of ultrafast laser techniques, femto/picosecond lasers have become an advanced tool for texturing materials. Periodic nanostructures were successfully produced on metals and semiconductors by picosecond laser irradiation [21,22]. The periodic structures self-form at the laser focusing spot and are perpendicular to the laser electric field polarization vector. The periodicity can be adjusted by the output of the laser. Although the mechanism of formatting the structure remained unclear, nanoplasma or surface instability that was generated by the femtosecond laser would be involved in the process [22,23]

In the present in-vitro study, the one-step laser ablation technique was explored to rapidly fabricate HMN structures on the commercial cobalt alloy using a picosecond Q-switched laser system. Various HMN structures were obtained on Co-Cr-Mo depending on the laser energy. Surface topographies were analyzed using a scanning microscope and 3D laser confocal microscope. The composites were evaluated by XRD and EDS. Behaviors of osteoblast cells on the HMN structured surfaces were investigated to evaluate the biocompatibility.

2. Materials and methods

Commercially available Cobalt–chromium–Molybdenum (Co–Cr–Mo) alloy (ASTM F75, Steel Material Technology Co., Ltd., China) was used as received and contained: C (≤0.35%), Mn (≤1.0%), Si (≤1.0%), Cr (26–30%), Ni (≤1%), Fe (≤0.75%), Mo (5.0-7.0%), Co (balance) and N (≤0.25%). The dimension of specimen was 12 mm × 6 mm × 2.5 mm. One 12 mm × 6 mm surface was polished to a mirror finish using a series of sand grinding papers up to 1600 grit. Then it was ultrasonic cleaned in ethanol and distilled water, following by drying in atmosphere. The surface roughness (Ra) ~80 nm was measured by a surface profiler (TR-200, Time Group) in a scanning length of 1.2 mm, which was consisted with the surface finish of the commercial hip joint replacements.

The picosecond Q-switched laser system (IC–1500 ps, Van laser) was used to fabricate hierarchical patterns on Co–Cr–Mo alloys. As shown in Fig. 1a, a typical line-by-line and serial process was performed to induce HMN structures. The laser beam (center wavelength: 800 nm; repetition: 1 kHz) was focus on the sample using a microscope lens with numerical aperture (NA) of 0.45 (Nikon, Japan). The shift of adjacent laser scanning line was kept constant,

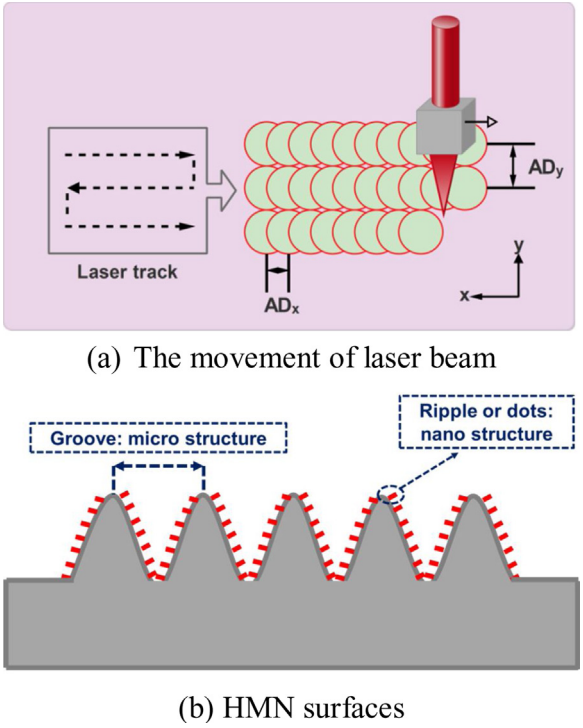

Fig. 1. Schematic illustration of the laser ablation process and HMN structures, (a) the moving path of laser beam and (b) the distribution of HMN structures.

25 μm, which was slightly larger than the diameter of MC3T3-E1 cell without spreading [24]. The laser machining platform was performed in ultraclean room under atmospheric conditions. In the irradiation, the wavelength (λ) of 1064 nm and 10 ps pulse length were used. After laser irradiation, periodic structures were fabricated on Co–Cr–Mo as shown in Fig. 1b. In terms of their periodicity, the topography can be divided into micro and nano structure. The micro structured groove had spatial periods of ~25 μm, which was equal to the shift of adjacent laser scanning line. The nano structures, such as ripples and islands, had spatial periods between 0.4 λ and λ. They were most likely produced by interaction between the incident laser beam and the surface scattered wave.

The power density of laser beam exhibited a Gaussian distribution. Usage of a shorter wavelength allowed smaller diffraction-limited spot sizes, which was favor in introducing finer features during the ablation process. Two types of power energy, such as 25 mW (12.7 J/cm^2) and 50 mW (25.4 J/cm^2, close to the threshold), were applied, which could produce two types of structures, denoted as HMN 25 and HMN 50, respectively.

The microstructure was observed by a SU3500 scanning electron microscope (JEOL, Japan) with an Oxford Inca energy dispersive X-ray microanalysis (EDX). Cross section profile was measured by 3D laser confocal microscope (OLS4000, Olympus). The phase composition of samples was characterized by X-ray diffraction apparatus (X'pert, Netherlands). The static contact angle (CA) was calculated by the sessile drop method using a JC2000D2A video based contact angle system (Powereach, China) according to Yong-Laplace fitting at room temperature. Experimental investigation for effect of the proposed HMN approach on the dynamic surface wettability was performed. During the measurement, water was continuously and slowly pumped into (or sucked from) the droplet. The evolution of the water droplet was recorded simultaneously. An advancing contact angle and a receding contact angle were calculated automatically. The contact angle hysteresis (CAH) was the difference between the advancing and the receding contact angle. CAH mea-

surements were performed at least four different positions for each surface.

The protein adsorption on samples was evaluated by AFM imaging. Procedures were performed as following. Firstly, samples were cleaned and incubated with phosphate buffer for 1 h. Secondly, phosphate buffer was removed and Bovine Serum Albumin (BSA, Sigma) solution with concentration of 2 mg/mL was added. After 30 min, the surface was rinsed to remove superfluous BSA solution. Finally, it was dried under clean atmosphere at room temperature. The Innova Digital Nanoscope AFM (Veeco, America) was used to investigate the topographic details. Commercial silicon microcantilever probes (RTESP, Bruker) with spring constant of 0.35 N/m and nominal tip radius of 8 nm were used in tapping mode. The scanning area was 2 μm × 2 μm with the scanning rate of 0.8 Hz.

Before and after laser ablation, the cytocompatiblity of Co–Cr–Mo alloy were evaluated by an in vitro assay. In all experiments, osteoblast precursor cells (MC3T3-E1) were seeded at a density of 5×10^4 cells/mL. Using 24-well culture plates, the MC3T3-E1cells were cultured in α-MEM medium containing 10 vol% fetal bovine serum and 1 vol% penicillin–streptomycin. The medium was changed every two days. The activity of MC3T3-E1 cells cultured on different samples was determined with 3-(4, 5-dimethylthiazol-2-yl)-2, 5-diphenyl tetrazolium bromide (MTT) colorimetric assay. After incubation for 6 h, 24 h and 48 h, they were rinsed twice with phosphate buffered saline (PBS). Subsequently, fresh α-MEM medium and MTT was added. The samples were incubated for another 4 h at 37 °C to form MTT formazan. Medium was replaced with dimethyl sulfoxide (DMSO, Sigma) and placed on a shaking bed for 10 min to dissolve the formazan crystals. Finally, 100 μL of the reacted reagent was transferred to 96-well plate and the absorbance was measured at 492 nm using a microplate spectrophotometer (DNM-9602). Morphologies of cells on the textured surface were observed by a fluorescence microscope (Nikon, Japan) after staining. The procedure of cell staining could be found in the previous work [25]. Cell nuclear aspect ratios and nuclear alignment were analyzed using the FIJI's best-fit ellipse tool. Feret diameters (max and min caliper distance) for cells not in contact with other cells were measured from actin images (FIJI) and used to analysis cell elongation ($Feret_{max}/Feret_{min}$) and alignment ($Feret_{max}$ orientation relative to pattern). All data was presented as mean ± standard deviation. Statistical analysis was performed using one-way analysis of variance following multiple comparisons with Ryan's test.

3. Results and discussion

3.1. Surface topography

SEM evaluation of the surface morphology is presented in Fig. 2 Before the laser irradiation, there were no structural features on the polished surface (Fig. 2a and d). After laser irradiation, it was covered by various non-smooth units. Two surface features were observed, periodic wave-like grooves (pitch around 25 μm and determined by the vertical shift of the laser path) and nano ripples (142 ± 52 nm in lateral width, Fig. 2e and f). With more energy irradiation, the volume of the periodic unit was increasing. Micropores, cluster of holes smaller than the laser beam spot size, appeared at the same time (HMN 50 samples). It indicated that laser fluence dependence of nano structure formation in Co-Cr-Mo alloy. With laser treatments, the height distribution was becoming widely (Fig. 2g). Surface roughness (Ra) was increased from 0.08 ± 0.02 μm for polished sample to 2.4 ± 1.2 μm for HMN25 and 3.3 ± 1.4 μm for HMN50 (Fig. 2h). The HMN 50 sample showed the highest surface roughness. The results showed that an interesting feature of the periodic groove decorating with nano-roughness structures was

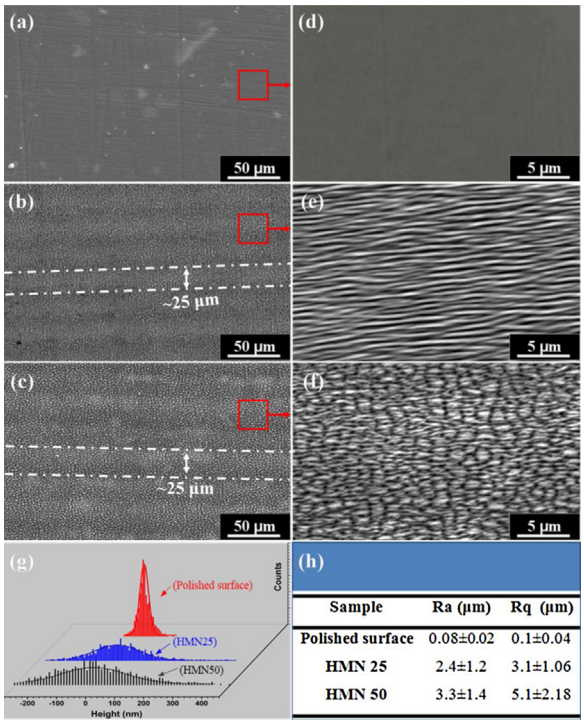

Sample	Ra (μm)	Rq (μm)
Polished surface	0.08±0.02	0.1±0.04
HMN 25	2.4±1.2	3.1±1.06
HMN 50	3.3±1.4	5.1±2.18

Fig. 2. SEM images of Co-Cr-Mo alloy samples with different laser irradiation energy: (a) Polished surface, (b) 25 mW and (c) 50 mW. High magnification SEM images of (a), (b) and (c) are shown in (d), (e) and (f), respectively. The histogram represents the vertical height distribution (g). (h) shows the Ra and Rq value for different samples. For Ra and Rq calculation, three different places for each sample were detected.

produced with the synergistic effect of laser movement and interference. It is in contrast to rectangular surface grooves fabricated using lithography techniques that usually have vertical ridges and rough floors. With exhibiting large amount of nano structure, nano structured materials had been regarded to process an increased numbers of atoms and crystal grains at the interface. Commonly, the adsorption of protein was significantly enhanced by the nano structure. Results of BSA AFM morphologies showed HMN structure induced a thicker layer of protein, which confirmed the effect of promoting adsorption on HMN surfaces (Fig.S1). Thus, following steps such as cell proliferation and differentiation may be promoted with the increase of protein adsorption.

For quantitative measurement of these hierarchical micro/nano surface structures, detailed cross-section profile was measured by 3D laser confocal microscope. The surface profile was analyzed for a cross section transverse to the micro grooves, which indicated the pitch of groove was equal to the shift of laser beam (25 μm). Fig. 3b and c showed the HMN roughened surface and height variations. The vertical depth of these nanoscale structures were in the range of 200–1000 nm. The surface morphologies on the Co-Cr-Mo surface with the picosecond laser irradiation were found to be similar and comparable with the commercially pure titanium with femtosecond laser pulses by Vorobyev and Guo [26]. The periodicity of these nanoscale structures is dependent on several factors and warrants detailed investigation. In general, it is equal to or less than wavelength λ of the laser beam. Due to the very short time scale involved in the laser ablation, the process can be considered as a direct solid-vapor or solid-plasma transition. The lattice was heated on a picosecond time scale which results in the creation of vapor and plasma phases followed by a rapid expansion. Formation of sub-wavelength ripples has also been observed and was attributed to the relaxation of highly excited unstable surface layers. The physical phenomena explaining the ripple initiation,

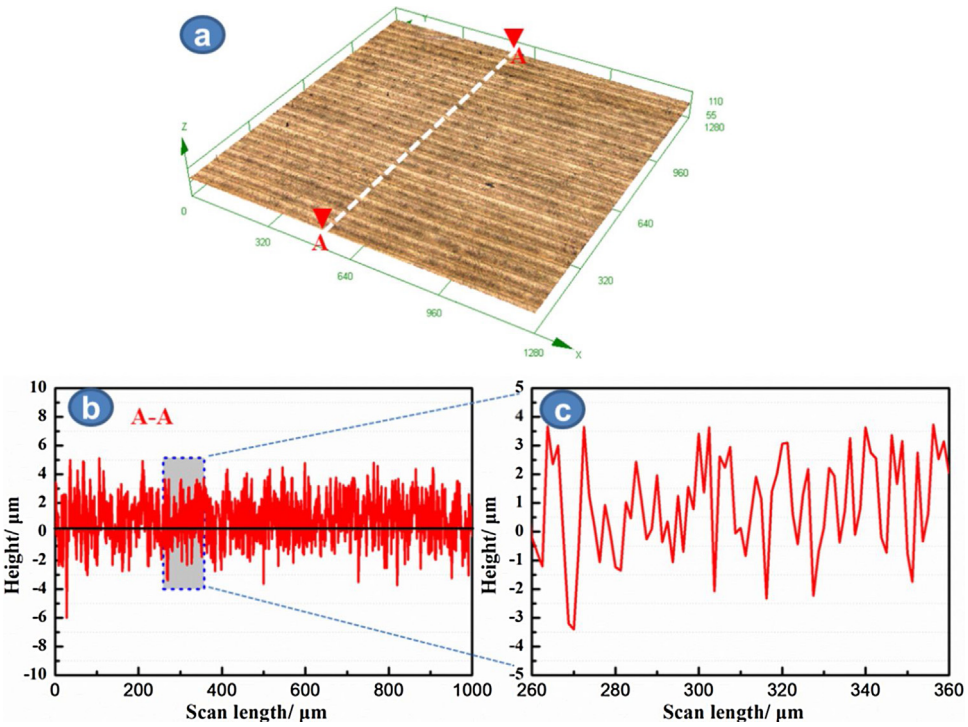

Fig. 3. The surface topography of HMN 25: (a) the 3D confocal image in a scanning size of 1000 µm × 1000 µm, (b) the corresponding cross sectional profile of white marked line A–A in (a) and (c) enlarged cross sectional profile of gray square in (b).

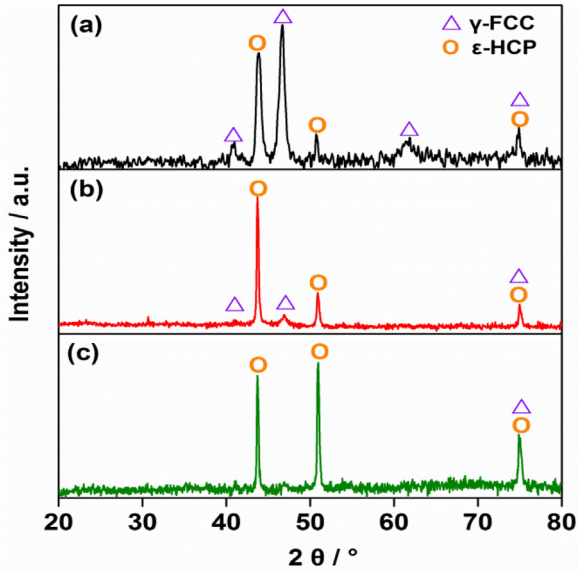

Fig. 4. XRD patterns of (a) Polished Co-Cr-Mo, (b) HMN25 and (c) HMN 50. Peaks at 41.3° and 47.3° are presented for (1 0 0) FCC and (1 0 1) FCC, respectively. Peaks at 44.2° and 51.1° are presented for (1 1 1) HCP and (2 0 0) HCP, respectively.

growth, and transition toward other patterns are still not clear. Further investigation is underway to understand the exact mechanism of micro/nano structure formation and their self-organization.

3.2. Surface composition

The XRD patterns of the laser melted surface are shown in Fig. 4. XRD peaks originated from γ- face-centered cubic structure (FCC) and ε-hexagonal closest packing structure (HCP) phases are observed. The intensities of (2 0 0) HCP peak at 51.1° and (1 0 1) FCC peak at 47.3° are used to estimate the relative amount of ε- and γ-phase, respectively [27]. For the laser irradiation samples, the intensity of HCP peak is increased while FCC peak is decreased as compared to non-treated samples. X-ray diffraction results show phase transformation connected to the laser irradiation. In our samples, the local molten area rapidly solidifies and cools down due to the high thermal conductivity of metallic alloy and smallness of the heated area. The production process is possible to reach very similar condition to the thermal martensitic transformation. Thus, Cobalt-based alloys undergo an FCC to HCP martensitic transformation [28]. The EDS analysis confirms that there is no substantial incorporation of any other element either during or after the ultrafast laser texturing process (See Fig. S2). The main peaks identified in the analysis are chromium between 5 and 6 keV and cobalt near 7 keV. When the laser spot was irradiated on the surface, the bulk material at the center of the laser irradiated zone would be ablated due to the relatively high laser intensity. Following processes such as phase explosion, ejection, and removal were caused by accumulated laser irradiation dose. It was reported that Ni concentration would be enriched on the surface in the heat treatment process. This was due to the supply of oxygen to the depth and Ni diffusion from the bulk to the surface of nitinol was observed [29]. On the laser irradiated Co-Cr-Mo surface, nano-plasma and/or local heat generated by the picosecond laser would have similar effect in supplying oxygen and inducing metal composite to the surface. As shown in Fig. S2, compared to unpatterned surface, bulk composite of Co and Mo (wt.%) for HMN surface was increased from 63.8 to 64.6 and 3.8–6.3, respectively. The Mo content was decreased probably due to its chemical reactivity lower than Co and Mo.

3.3. Surface wettability

Contact angle measurements were used to evaluate the wettability of the different surfaces by calculating the shape of a water drop resting on horizontal surface. Fig. 5 shows the results of static water contact angle measurements on the Co–Cr–Mo surfaces with and without laser irradiation. It was observed that the wettabil-

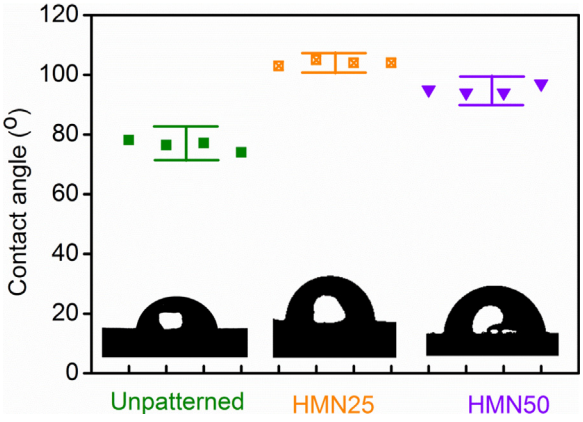

Fig. 5. The effect of the laser irritation on the water contact angles of Co-Cr-Mo surfaces. Four samples from each treated groups were used for the measurements. Three different places were selected to make sure the homogeneity of every sample.

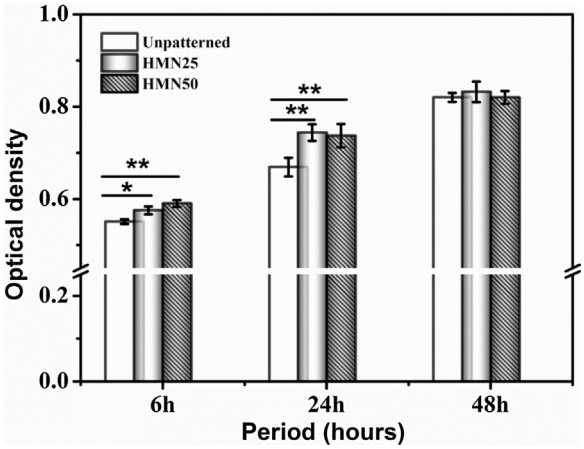

Fig. 6. Proliferation of MC3T3-E1 cells cultured on HMN samples at different time interval. The data represent the mean ±SD, *P < 0.05 and **P < 0.001 ((multiple comparison analysis).

ity was significantly changed after laser irradiation. The contact angle of the smooth surface was 76.4° ± 1.7°, while HMN surfaces had higher contact angles, 104° ± 0.8 °for HMN 25 and 95° ± 1.4 °for HMN50. Contact angle measurements reveal that the HMN structures, varying the power of laser, have direct impact on the wate

r repellence properties. As the roughness increases, the water droplets contact only with the peaks and/or nanoscale ripples on the laser machined surface. This creates additional liquid-air interface rather than entire liquid-solid interface. The enhancement in water repellence of these substrates can be attributed to dual-scale surface roughness[30]. Wetting behaviors with fluids can be influenced by surface topographies. In this study, HMN structures exhibited higher contact angles than the unpatterned surface. The wetting with water was influenced by the anisotropy of the structures, as the structural elevations acted as energy barriers and blocked the spreading of water. Thereby, higher contact angle values were observed for HMN surfaces.

As shown in Fig. S3, the CAHs measured on the HMN 25 and HMN 50 were 32.6 ± 6.1° and 44.8 ± 8.3°, respectively. The polished surface showed the highest CAH, 50.4 ± 12.9°. Compared to HMN 25, the CAH of HMN 50 was increased but still less than the polished surface. This was due to interruption and vanishing of the elongated nanoripples with higher laser energy and thus the real contact area between the water droplet and surface was decreased. Results indicated that the nanoripples on the micro-structures can make it possible to enhance the surface wetting properties and provide the sufficient air-trappable sites.

3.4. Cell proliferation

Fig. 6 presents the proliferation of MC3T3-E1 cells on the laser ablation samples. Three different incubation intervals were used, such as 6, 24 and 48 h. Optical density was increased for all samples as time prolonging. For the initial 6 h, the proliferation was slightly increased (around 4.1%) on HMN25 samples and it was significantly increased on HMN50 (around 7.2%) as compared to that of the unpatterned sample. The first 6 h was always regarded as the period of the cell adhesion. It was mainly was associated with the surface roughness and the highest roughness HMN50 showed the highest value of optical density. After 24 h, both of HMN 25 and HMN 50 samples have a significantly improvement in the proliferation of osteoblast cells compared to the unpatterned sample. It was increased 11.2% for HMN 25 and 10.8% for HMN 50. After culturing 48 h, no significant difference among three samples was observed. According to previous studies, osteoblast cells were influenced by the surface roughness both at microscale and nanoscale. Huang investigated the effects of hierarchical micro/nano-topographies on the response of cells and results showed that nanoplate surface slowed down cell proliferation, while nanoleaf surface supported it [31]. Yiannakou's results indicated cells were repelled with nano ripples alone while they were promoted on micro and nano topographies. Our results showed the same synergy effect of HMN structures on cell proliferation. However, the effect of HMN structures on improving cell activity was restricted for 48 h and this was probably due to the spatial limitation of crowding cells. Results indicate topography-induced effects are primary factors in the initial period of cell–substrate contact and the bioactivity of the laser ablation treated surface could be highly improved by forming a hierarchical structure.

Although wettability is generally thought to be involved in cell attachment and spreading, the best value of contact angle for cell attachment and spreading is still uncertain. In addition to the difference in surface topology, the water droplet size effects on the contact angles should be considered [32]. Kosuke Nozaki studied the wetting behavior and cell spreading on the structured nitinol surface. Even with contact angle increasing, the cell alignment was still improved while platelets failed to adhere on hydrophobic surfaces. Results indicated that hydrophobic surface would inhabit the attachment of small units but large units, e.g. cells, may be not restricted by this problem [33].

3.5. Influence of surface topography on cell morphology

The orientation of cells on the specimens was evaluated using cell angles, as assessed by the cellular outline and direction of the nuclei and cytoskeleton in 100 microscopically imaged cells. MC3T3-E1 cells on the HMN surface exhibited an elongated morphology and were aligned along with the direction of the grooved surface (Fig. 7). In contrast, neither elongation nor orientation was founded among MC3T3-E1 cells on unpatterned surfaces (Fig. 7a). The aspect ratio of cells on HMN substrates was almost twice than cells on unpatterned substrates. The F-actin fiber was found to be mostly stretched along the long axis of cells. HMN 25 presented a narrow distribution of cells between 0 and 15° on cell orientation while HMN 50 presented a broader distribution between 0 and 35° (Fig. 7b). Similarly, nuclei of cells on HMN25 were found to have higher alignment with the pattern direction (Fig. 7c). It was reported that nucleus was mechanically integrated with the physical entity of cell via intermediate filaments [34]. Active or passive cell extension can lead to passive nuclear deformation. In the study, cell elongation was both significantly regulated by HMN 25

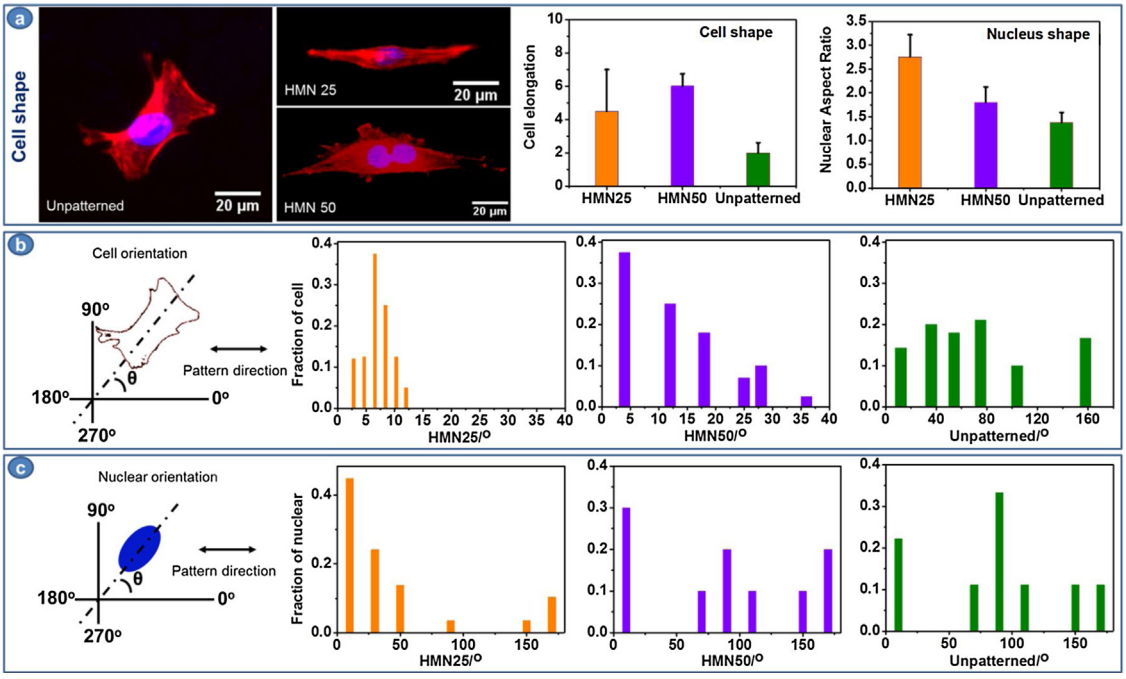

Fig. 7. HMN architecture directs alignment and changes shape of single osteoblast. (a) The cell elongation and cell nuclear aspect ratio was measured after 6 h attachment. (b) Exhibited higher cell orientation compared to unpatterned surface. (c) On HMN surface, cell nuclear was significantly more aligned with the pattern direction.

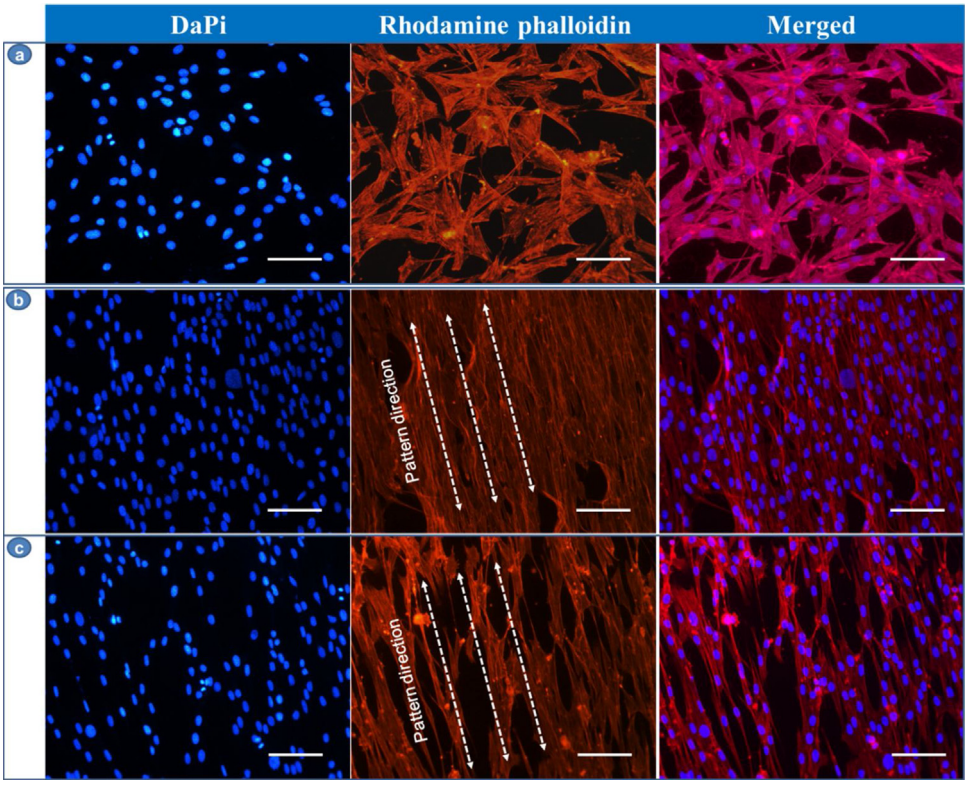

Fig. 8. Fluorescence microscope images of cultured MC3T3-E1 cells after seeding 48 h. (a) Polished Co-Cr-Mo, (b) HMN25 and (c) HMN 50. From left to right, nuclear stained, actin stained and the two merged were presented, respectively.

and HMN 50, while elongated cells (cell area) were dominating on HMN25 as compared to cells on HMN 50. Therefore, higher nuclear aspect was observed on HMN 25.

Recently, it was found that an engineered substratum could play a key role in regulating cell differentiation. The cell morphology has been described as an indicator of the commitment toward osteoblastic lineage [35]. Round or polygon shaped cells were associated with adipogenic differentiation, while elongated shaped cells as observed on the patterned surface may promote osteogenic transition. Additionally, controlling the spatial arrangement of different cells paves the way for the development of patterned co-cultures, especially when they are kept separately

at the same time. Such co-cultures enable the precise control of homotypic and heterotypic contact.

To investigate the effect of HMN structure on groups of cells, osteoblast cells were seeded at higher densities (8×10^4 cells/mL) on the patterned substrates and cultured for 48 h. As shown in Fig. 8, the number of osteoblast cells on HMN Co–Cr–Mo alloy was significantly more than controls and there was different cell response and outgrowth on the various substrates. With the laser irradiation, which resulted in combined micro- (grooves) and nano- (ripples) roughness, cell outgrowth was significantly improved and highly oriented. For HMN25, cells were guided with the microgrooves and exhibiting similar periodicity to that of the nanorippled substrates. For HMN50, cells were more likely to be pinned at the corner of "micro islands" while were still aligned with the direction of microgroove. The above results demonstrate the significant role of hierarchical morphology, i.e. the combination of micro- and nano- features, on favoring cell outgrowth. It suggests a fascinating strategy for achieving quick and mechanically stable anchoring of cells due to the synergetic effect of micro- and nano-scale surface roughness.

The study of interactions between cells and substrate in vitro can better mimic complexity of the in vivo cellular microenvironment [36]. Substrates with grooves have been used to promote cell contact guidance, phenomenon that cells align themselves and migrate along the grooves. This has been shown to reduce the extent of scar tissue formation and promote osseointegration. Efforts have been made into unraveling the underlying mechanisms of contact guidance and several theories have also emerged on experimental research[37]. Other engineering approaches were implemented to control the spatial arrangement of cells in order to generate patterned co-cultures [38]. However, most of these approaches were mainly based on the differential preference of the various cells to specific ECM molecules, which was mainly rely on the chemical composite of the substrate. In this research, we investigated the response of osteoblast cell to combinations of cell adhesive architecture at two distinctly length scales (micro-scale groove-like architecture and nano-scale geometric confinement). Usually, cells are resided in a complex environment that has a high degree of structural organization. This is well illustrated in the hierarchical structural arrangement of different cells in human body [39]. Topographies used in the study, e.g., microgrooves and oriented nanostructures, were similar to the geometry of bone found in vivo. In the microscale, the lamellar bone is constituted of units called osteon. Each osteon contains several layers of concentric lamellae which are in the scale of around 20 μm. The concentric lamellae can be likened to the microgrooves. In the nanoscale, the collagen fibrils have defined structures inside each lamella [40,41]. Oriented nano ripples inside the microgrooves were close to this organization. As presented in the work, the remarkable dependence of cell outgrowth may realize controllable cellular patterns onto one single culture substrate. As an example, the desired pattern that comprises interfaces of CR (cell-random) with flat and/or CG regions (cell-guidance/orientation) may be easily realized, which will help us reveal the mechanisms behind cell adhesion, sensing and differentiation.

4. Conclusions

In summary, using one step laser ablation technique, grooved surfaces with micro and nano structure were rapidly fabricated onto Co-Cr-Mo alloy. The interesting result of this study is that the ridges and the grooves of the periodic structures produced with picosecond laser are extensively covered with nanoscale structures. As the surface undergoes repeated pulses per irradiated spot, because of the melting and ejection of liquid to the periphery of the melt region, results in HMN structures. MC3T3-E1 cells cultured on the surface with HMN structured surface was exhibited an elongated morphology and aligned along with the pattern direction. Meanwhile, enhanced osteoblast adhesion and improved cell proliferation were found on HMN surfaces. These findings highlight the importance of guidance cues/synergetic effect at multiple length scales, which have potential applications in controlling tissue organization and considerable importance for the orthopedic implants, in particular osseointegration.

Acknowledgments

The authors acknowledge the joint financial support from the National Natural Science Foundation of China (51605370, 51475358 and 51675409), the Natural Science Fund of Shaanxi Province (2017JQ5009) and China Postdoctoral Science Foundation funded project (2016M602802). We thank Mr Ren at instrument analysis center of Xi'an Jiaotong University for his assistance with SEM analysis.

Appendix A. Supplementary data

Supplementary data associated with this article can be found, in the online version, at https://doi.org/10.1016/j.colsurfb.2017.11.040.

References

[1] B.-S. Kim, I.-K. Park, T. Hoshiba, H.-L. Jiang, Y.-J. Choi, T. Akaike, C.-S. Cho, Design of artificial extracellular matrices for tissue engineering, Prog. Polym. Sci. 36 (2011) 238–268.
[2] K.B. Fonseca, P.L. Granja, C.C. Barrias, Engineering proteolytically-degradable artificial extracellular matrices, Prog. Polym. Sci. 39 (2014) 2010–2029.
[3] J. Park, S. Bauer, K.A. Schlegel, F.W. Neukam, K. von der Mark, P. Schmuki, TiO2 nanotube surfaces: 15 nm – an optimal length scale of surface topography for cell adhesion and differentiation, Small 5 (2009) 666–671.
[4] K.S. Katti, Biomaterials in total joint replacement, Colloids Surf. B: Biointerfaces 39 (2004) 133–142.
[5] Y. Sato, N. Nomura, A. Chiba, Effect of nitrogen content on microstructure of hot-pressed Co-Cr-Mo alloy compacts for biomedical applications, J. Jpn. Inst. Met. 72 (2008) 875–880.
[6] R.A. Gil, A.I. Munoz, Influence of the sliding velocity and the applied potential on the corrosion and wear behavior of HC CoCrMo biomedical alloy in simulated body fluids, J. Mech. Behav. Biomed. Mater. 4 (2011) 2090–2102.
[7] S. Zangeneh, H.R. Lashgari, A. Roshani, Microstructure and tribological characteristics of aged Co-28Cr-5Mo-0.3C alloy, Mater. Des. 37 (2012) 292–303.
[8] H. Zhang, L. Blunt, X. Jiang, L. Brown, S. Barrans, Y. Zhao, Femoral stem wear in cemented total hip replacement, Proceedings of the Institution of Mechanical Engineers, Part H, J. Eng. Med. 222 (2008) 583–592.
[9] L. Qin, H. Dong, Z. Mu, Y. Zhang, G. Dong, Preparation and bioactive properties of chitosan and casein phosphopeptides composite coatings for orthopedic implants, Carbohydr. Polym. 133 (2015) 236–244.
[10] J.R. Bush, B.K. Nayak, L.S. Nair, M.C. Gupta, C.T. Laurencin, Improved bio-implant using ultrafast laser induced self-assembled nanotexture in titanium, J. Biomed. Mater. Res. B Appl. Biomater. 97 (2011) 299–305.
[11] W. Liu, X. Liu, J. Fangteng, S. Wang, L. Fang, H. Shen, S. Xiang, H. Sun, B. Yang, Bioinspired polyethylene terephthalate nanocone arrays with underwater superoleophobicity and anti-bioadhesion properties, Nanoscale 6 (2014) 13845–13853.
[12] C. Liu, Q. Zhang, T. Li, Z. Li, Superoleophobic and superhydrophobic surfaces from microtextured znO-Based surfaces on Si substrate, in: W. Pan, J. Gong (Eds.), High-Performance Ceramics Vi, 434-435, 2010, pp. 538–541.
[13] S. Wu, X. Liu, K.W. Yeung, C. Liu, X. Yang, Biomimetic porous scaffolds for bone tissue engineering, Mater. Sci. Eng. R: Rep. 80 (2014) 1–36.
[14] N.D. Gallant, J.L. Charest, W.P. King, A.J. Garcia, Micro- and nano-patterned substrates to manipulate cell adhesion, J. Nanosci. Nanotechnol. 7 (2007) 803–807.
[15] K. Kolind, K.W. Leong, F. Besenbacher, M. Foss, Guidance of stem cell fate on 2D patterned surfaces, Biomaterials 33 (2012) 6626–6633.
[16] K. Kulangara, Y. Yang, J. Yang, K.W. Leong, Nanotopography as modulator of human mesenchymal stem cell function, Biomaterials 33 (2012) 4998–5003.
[17] X. Lu, Y. Leng, Quantitative analysis of osteoblast behavior on microgrooved hydroxyapatite and titanium substrata, J. Biomed. Mater. Res. A 66A (2003) 677–687.

[18] H.-A. Pan, Y.-C. Hung, J.-C. Chiou, S.-M. Tai, H.-H. Chen, G.S. Huang, Nanosurface design of dental implants for improved cell growth and function, Nanotechnology 23 (2012) 335703.
[19] T.J. Webster, C. Ergun, R.H. Doremus, R.W. Siegel, R. Bizios, Enhanced functions of osteoblasts on nanophase ceramics, Biomaterials 21 (2000) 1803–1810.
[20] J. Yong, F. Chen, Q. Yang, G. Du, C. Shan, H. Bian, U. Farooq, X. Hou, Bioinspired transparent underwater superoleophobic and anti-oil surfaces, J. Mater. Chem. A 3 (2015) 9379–9384.
[21] M. Tsukamoto, K. Asuka, H. Nakano, M. Hashida, M. Katto, N. Abe, M. Fujita, Periodic microstructures produced by femtosecond laser irradiation on titanium plate, Vacuum 80 (2006) 1346–1350.
[22] S.K. Das, D. Dufft, A. Rosenfeld, J. Bonse, M. Bock, R. Grunwald, Femtosecond-laser-induced quasiperiodic nanostructures on TiO2 surfaces, J. Appl. Phys. 105 (2009) 084912.
[23] G. Miyaji, K. Miyazaki, K. Zhang, T. Yoshifuji, J. Fujita, Mechanism of femtosecond-laser-induced periodic nanostructure formation on crystalline silicon surface immersed in water, Opt. Express 20 (2012) 14848–14856.
[24] L. Qin, Q. Zeng, W. Wang, Y. Zhang, G. Dong, Response of MC3T3-E1 osteoblast cells to the microenvironment produced on Co–Cr–Mo alloy using laser surface texturing, J. Mater. Sci. 49 (2014) 2662–2671.
[25] E. Lamers, R.V. Horssen, J.T. Riet, F.V. Delft, R. Luttge, X. Walboomers, J. Jansen, The influence of nanoscale topographical cues on initial osteoblast morphology and migration, Eur. Cells Mater. 20 (2010) 329–343.
[26] A.Y. Vorobyev, V.S. Makin, C. Guo, Periodic ordering of random surface nanostructures induced by femtosecond laser pulses on metals, J. Appl. Phys. 101 (2007) 034903.
[27] S. Hiromoto, E. Onodera, A. Chiba, K. Asami, T. Hanawa, Microstructure and corrosion behaviour in biological environments of the new forged low-Ni Co-Cr-Mo alloys, Biomaterials 26 (2005) 4912–4923.
[28] A. Garcia, A.M. Medrano, A.S. Rodriguez, Formation of Hcp martensite during the isothermal aging of an Fcc Co-27Cr-5Mo-0.05C orthopedic implant alloy, Metal. Mater. Trans. a-Phys. Metall. Mater. Sci. 30 (1999) 1177–1184.
[29] S.A. Shabalovskaya, J. Anderegg, F. Laab, P.A. Thiel, G. Rondelli, Surface conditions of Nitinol wires, tubing, and as-cast alloys. The effect of chemical etching, aging in boiling water, and heat treatment, J. Biomed. Mater. Res. B Appl. Biomater. 65 (2003) 193–203 (B).
[30] D.M. Spori, T. Drobek, S. Zuercher, M. Ochsner, C. Sprecher, A. Muehlebach, N.D. Spencer, Beyond the lotus effect: roughness influences on wetting over a wide surface-energy range, Langmuir 24 (2008) 5411–5417.
[31] Q. Huang, T.A. Elkhooly, X. Liu, R. Zhang, X. Yang, Z. Shen, Q. Feng, Effects of hierarchical micro/nano-topographies on the morphology, proliferation and differentiation of osteoblast-like cells, Colloids Surf. B: Biointerfaces 145 (2016) 37–45.
[32] Y.C. Jung, B. Bhushan, Wetting transition of water droplets on superhydrophobic patterned surfaces, Scr. Mater. 57 (2007) 1057–1060.
[33] K. Nozaki, T. Shinonaga, N. Ebe, N. Horiuchi, M. Nakamura, Y. Tsutsumi, T. Hanawa, M. Tsukamoto, K. Yamashita, A. Nagai, Hierarchical periodic micro/nano-structures on nitinol and their influence on oriented endothelialization and anti-thrombosis, Mater. Sci. Eng.: C 57 (2015) 1–6.
[34] A.J. Maniotis, C.S. Chen, D.E. Ingber, Demonstration of mechanical connections between integrins cytoskeletal filaments, and nucleoplasm that stabilize nuclear structure, Proc. Natl. Acad. Sci. U. S. A. 94 (1997) 849–854.
[35] A. Tijore, P.Q. Cai, M.H. Nai, Z.Y. Li, W. Yu, C.Y. Tay, C.T. Lim, X.D. Chen, L.P. Tan, Role of cytoskeletal tension in the induction of cardiomyogenic differentiation in micropatterned human mesenchymal stem cell, Adv. Healthc. Mater. 4 (2015) 1399–1407.
[36] H. Kaji, G. Camci-Unal, R. Langer, A. Khademhosseini, Engineering systems for the generation of patterned co-cultures for controlling cell–cell interactions, Biochimica et Biophysica Acta (BBA) 1810 (2011) 239–250 (General Subjects).
[37] C. Cammuso, C. Porter, S. Nims, D. Gaucher, D. Melican, S. Bombard, N. Hawkins, A. O'Coin, C. Ricci, C. Brayman, N. Buzzell, C. Ziomek, W. Gavin, Hormonal induced lactation in transgenic goats, Anim. Biotechnol. 11 (2000) 1–17.
[38] K.A. Kilian, B. Bugarija, B.T. Lahn, M. Mrksich, Geometric cues for directing the differentiation of mesenchymal stem cells, Proc. Natl. Acad. Sci. 107 (2010) 4872–4877.
[39] K. Anselme, B. Noël, P. Hardouin, Human osteoblast adhesion on titanium alloy stainless steel, glass and plastic substrates with same surface topography, J. Mater. Sci. 10 (1999) 815–819.
[40] B.S. Zhu, Q.H. Lu, J. Yin, J. Hu, Z.G. Wang, Alignment of osteoblast-like cells and cell-produced collagen matrix induced by nanogrooves, Tissue Eng. 11 (2005) 825–834.
[41] X.F. Walboomers, H.J.E. Croes, L.A. Ginsel, J.A. Jansen, Contact guidance of rat fibroblasts on various implant materials, J. Biomed. Mater. Res. 47 (1999) 204–212.